Small-angle neutron scattering quantification of phase separation and the corresponding embrittlement of a super duplex stainless steel after long-term aging at 300C

Journal Item

Materialia 000 (2020) 100771

Contents lists available at ScienceDirect

Materialia

journal homepage: www.elsevier.com/locate/mtla

Full Length Article

Small-angle neutron scattering quantification of phase separation and the corresponding embrittlement of a super duplex stainless steel after long-term aging at 300°C

Yadunandan Das[a,b,*], Jianling Liu[a], Sten Wessman[c], Xin Xu[d], Joakim Odqvist[a], Stephen King[e], Peter Hedström[a,*]

[a] Department of Material Science and Engineering, KTH Royal Institute of Technology, SE-100 44 Stockholm, Sweden
[b] Presently at: The Open University, Walton Hall, Milton Keynes MK7 6AA, United Kingdom
[c] Swerim AB, Kista, Stockholm, SE-164 07, Sweden
[d] Department of Materials, Imperial College London, SW7 2AZ, United Kingdom
[e] ISIS Pulsed Neutron & Muon Source, Rutherford Appleton Laboratory, Didcot OX11 0QX, United Kingdom

ARTICLE INFO

Keywords:
Small-angle scattering (SAS)
Neutrons
Duplex stainless steel (DSS)
Phase transformation
Phase separation
Spinodal decomposition
475°C embrittlement

ABSTRACT

Small-angle neutron scattering (SANS) was applied to quantify the nanostructural evolution during spinodal decomposition in a 25Cr-7Ni (wt.%) super duplex stainless steel isothermally aged at 300 °C, for up-to 48,000 h. Prior to the application on the 25Cr-7Ni alloy, the SANS methodology was validated by comparing results from SANS measurements on binary Fe-Cr alloys with atom probe tomography results. SANS results on the 25Cr-7Ni alloy indicated that decomposition wavelength decreased from 5.1 nm to 4.5 nm, whereas the amplitude increased from 15.0 to 33.4 at.%. This quantitative nanostructural evolution correlated to a hardening of the ferrite phase by 190 HV and a reduction of the sub-size Charpy-V impact toughness from 60 J to 25 J.

1. Introduction

Phase separation in Fe-Cr alloys has been investigated extensively because Fe-Cr is the base system for the important stainless steel alloy category [1–7]. During the aging of Fe-Cr alloys, containing the ferrite or the martensite phase, at intermediate and low temperatures, phase separation occurs with the development of nanostructural Fe-rich (α) and Cr-rich (α') domains owing to the immiscibility of these two elements [8]. Depending on the chemical composition of the alloy and the temperature of aging, the phase separation progresses either by nucleation and growth or spinodal decomposition [9]. This phase separation can lead to the phenomenon of '475 °C embrittlement'. Since the embrittlement phenomenon limits the application of important stainless steel alloys, such as duplex stainless steels (DSS), the evolution of the nanostructure (and the consequential embrittlement) has been of interest for a long time [10–22].

Although quantitative information of the phase separation phenomenon may be obtained from techniques such as atom probe tomography (APT) [1,10,11], this information is localised and requires extensive sample preparation. Phase separation may also be studied by small-angle scattering techniques such as small-angle X-Ray scattering (SAXS) [23,24] or small-angle neutron scattering (SANS). Neutrons provide a significantly stronger contrast between Fe and Cr than X-rays unless the anomalous SAXS (ASAXS) technique is used [23,24]. A general benefit of the small-angle scattering techniques, in particular SANS, over many other characterization methods is the larger probe volume providing significant measurement statistics. Therefore, this manuscript explores an approach where SANS data is used to quantitatively study the amplitude (difference in Cr concentration between the α and α' domains) and wavelength (distance between two α' domains) evolution during phase separation. This manuscript first describes the SANS methodology applied for quantification of the nanostructural features developing during the α and α' phase separation. In order to validate the approach, SANS results were compared to quantifications based on APT data for binary Fe-Cr alloys. Thereafter, SANS was applied to quantify the nanostructure evolution for a 25Cr-7Ni (wt.%) super DSS (UNS S32750). The upper service temperature of, for example, pressure vessels made of grades 22Cr-5Ni, 23Cr-4Ni and the alloy studied here 25Cr-7Ni is 250 °C according to the EN standard, whilst it is 316 °C in ASME Section VIII Div 1-I. It should also be noted that accelerated aging (*i.e.*, aging at higher temperatures) may activate other phase decomposition mechanisms, and would therefore not be directly comparable to aging at the service temperatures. For

* Corresponding authors: Department of Material Science and Engineering, KTH Royal Institute of Technology, SE-100 44 Stockholm, Sweden.
E-mail addresses: ydas@kth.se, yadunandan.das@gmail.com (Y. Das), pheds@kth.se (P. Hedström).

https://doi.org/10.1016/j.mtla.2020.100771
Received 29 March 2020; Accepted 6 June 2020
Available online xxx

example, G-phase precipitation has been found to be more pronounced for accelerated aging conditions [25]. Therefore, here we conducted our long-term aging experiments at the technically relevant temperature of 300 °C.

The results of the nanostructure evolution in the present work are subsequently compared with data from hardness and impact energy testing to investigate how hardening and embrittlement correlates with the underlying nanostructure. The purpose of this paper is to lay the foundation for a systematic and extensive study correlating nanostructure evolution and associated embrittlement in DSS at industrially relevant service temperatures.

2. Experimental procedure

2.1. Materials and heat treatment

Outokumpu Stainless AB supplied 6 mm thick plates of 25Cr-7Ni super DSS with chemical composition in wt.%.: C (0.012), Si (0.3), Mn (0.83), Cr (24.84), Ni (6.90), N (0.28), Cu (0.18), Fe (balance). The Fe-Cr binary alloys with composition in wt.% (Cr = 25.3, 30.4, 36.1) were produced by vacuum arc melting and were fully ferritic [11]. Plates sized ~ 120 × 120 × 6 mm^3 of the 25Cr-7Ni super DSS were subjected to isothermal heat treatments at 300 °C for aging times of 3000, 6000, 12,000, 24,000 and 48,000 h. Whereas, the Fe-Cr alloy samples were heat treated at 500 °C for up to 1000 h.

2.2. Mechanical testing

Vickers micro-hardness testing was conducted on the section perpendicular to the rolling direction using a Qness Q10 micro-hardness indenter with a 5 g load. Prior to the hardness indentations austenite and ferrite phases were revealed by lightly etching the specimens in a solution of 100 ml HCl, 10 ml HNO_3 and 100 ml H_2O. For each isothermal aging condition, an average of 15 measurements were taken in both the austenite and ferrite phases.

Impact toughness was evaluated using an instrumented Instron tester – model 350MPX-V2. The test specimens were sub-size with dimensions 55 × 10 × 5 mm^3. The samples had the V-notch positioned in the rolling direction/transverse direction plane and were carried out at room temperature. Each specimen had a notch depth of 2 mm in accordance with the Swedish Standard [26].

2.3. Small-angle neutron scattering (SANS)

For SANS studies, all the specimens were prepared by cutting and polishing to dimensions ~ 10 × 10 × 1.5 mm^3. These samples were cut to shape using a Struers Accutom 5-disc cutter. Grinding and polishing were done using standard metallographic sample preparation techniques to remove any plastic deformation induced due to the cutting. Both sides of the SANS samples were ground and polished down to a grit size of 2500, removing about 100 μm from each side. SANS experiments were conducted at the *LOQ* diffractometer at the ISIS Pulsed Neutron and Muon Source, UK [27]. This is a "white beam" instrument that uses the time-of-flight technique to sort the arrival of different neutron wavelengths at the detectors. The incident beam aperture was set to 8 mm diameter. For the super DSS alloy, owing to the presence of a Bragg edge below 4.3 Å, only neutrons in the wavelength range of 4.3 – 10 Å were included in the data reduction [28]. In contrast, for the Fe-Cr alloys, as this effect was minimal, the full range of neutron wavelengths available, 2.2–10 Å, were used. Furthermore, the super DSS were measured with a saturating transverse magnetic field of 1.5 T, whereas the Fe_{1-x}-Cr_x alloys were measured without the application of this saturating magnetic field (measured in a separate SANS experiment by some of the present authors [29]). Data were reduced using the Mantid framework (version 4.2) [29,30,31] and a calibration standard, a solid blend of perdeuterated and hydrogeneous polystyrene, measured under the same

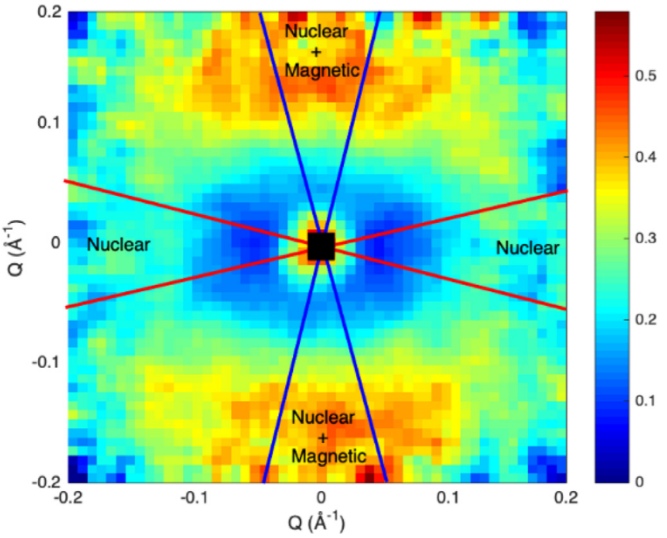

Fig. 1. Intensity map of the 2D scattering pattern of 25Cr-7Ni super DSS aged at 300 °C for 48,000 h with a saturating 1.5 T magnetic field applied horizontally, where the labels Nuclear and Magnetic denote the nuclear scattering and magnetic scattering contributions, respectively. Horizontal sector data was reduced from −20°- to +20°-degrees and the vertical sector data was reduced from +70° to +110°-degrees. In both cases the mirror sectors were included.

experimental conditions, was used to place the macroscopic coherent differential scattering cross section ($d\Sigma\ (Q)/d\Omega$), colloquially referred to as the intensity I, as a function of scattering vector ($Q = 4\ \pi\lambda^{-1} sin\ \theta$, where λ is the wavelength of incident neutrons and 2θ is the scattering angle) on an absolute scale in accordance with established procedures [32]. For the investigated super DSS, about 40.6 vol.% of the illuminated volume was the ferrite phase in which phase separation occurred and thus contributed to the correlation peak in the SANS data [28].

The total scattering obtained from SANS is a combination of scattering from nuclear ($I_{nuclear}$) and magnetic ($I_{magnetic}$) scattering contributions. When a saturating magnetic field, H, is applied (see Fig. 1), the total scattering becomes a function of the angle, Ψ, between the scattering vector and the direction of the applied field as follows:

$$I(Q)_{total} = I(Q)_{nuclear} + I(Q,H)_{magnetic}\ Sin^2\psi \quad (1)$$

Therefore, the scattering along the horizontal axis of the detector (where Ψ ~ 0° or 180°) should give the pure nuclear scattering contribution (being parallel to the direction of the applied field), whilst the scattering along the vertical axis (where Ψ ~ 90° or − 90°) should give a combination of nuclear plus magnetic scattering. This also implies that the magnetic contribution may be obtained by a simple subtraction of the horizontal scattering from the vertical scattering. This manuscript presents and discusses results only from analysis of the nuclear scattering contribution (integrated over the narrow range $-20° \le \Psi \le +20°$ and the mirror sector to improve the statistics) from the 25Cr-7Ni super DSS since the magnetic contribution is not negligible under the investigated conditions [33]. Prior to this discussion the applied SANS methodology is evaluated on SANS data for Fe-Cr alloys thermally aged at 500 °C, for up to 1000 h but measured in the absence of a saturating field, *i.e.* the total scattering is evaluated over the full range of azimuthal angles (Ψ = 0° to 360°). Since magnetic scattering is not negligible in the binary alloys studied here it was necessary to consider the relation between total and nuclear scattering in the analysis of the binary alloys. We discuss this in more detail in our Results and Discussion.

The SANS results are compared with APT measurements of wavelength and amplitude reported in Refs. [34] and [11]. In Pettersson et al. [34] the same 25Cr-7Ni super DSS (as in this work) was measured, but only for up to 12,000 h of aging at 300 °C.

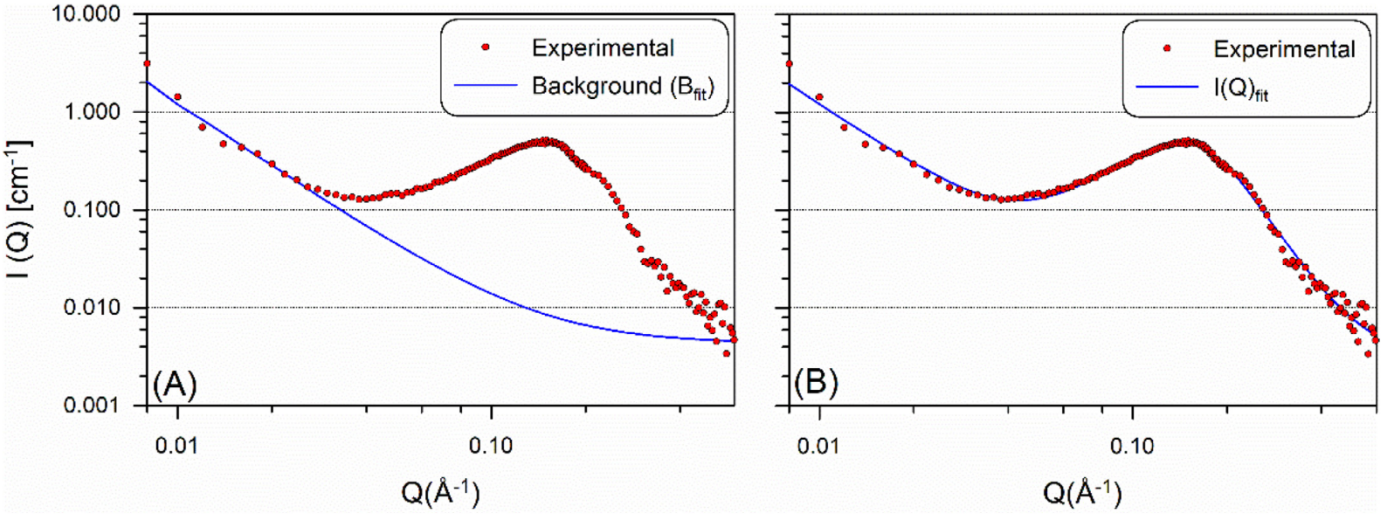

Fig. 2. Illustration of fitting (A) the background and (B) the complete scattering data. Model fitting parameters give wavelength and amplitude of phase separation. Data shown are 25Cr-7Ni super DSS isothermally aged at 300 °C for 48,000, fitting χ^2=3.0.

Using the SasView software (version 4.2.2) [35] a combination of a power law background function [14,36] and a generalised spinodal function [37] were fitted to the scattering data such that:

$$I(Q)_{fit} = B_{fit} + I(Q)_{spinodal} \quad (2)$$

where the term $B_{fit} = A_{power\_law}\, Q^{-n} + B_g$, n is the power law exponent ($1.5 \le n \le 4$), the A prefactor determine the relative contribution of each term, and B_g is the residual Q-independent background level (which mostly arises from incoherent scattering). Note that $I(Q)_{fit}$ and B_{fit} and $I(Q)_{spinodal}$all have dimensions of inverse length (here cm^{-1}), but the dimensions of A_{power_law} will vary with n.

The power law part of the model is simply used to accurately fit the background underlying the scattering curve (denoted B_{fit} in Fig. 2), whereas the scattering peak arising from phase separation, here assumed to arise due to spinodal decomposition, is fitted using the spinodal model. Note that the background comprises both Q-dependent and Q-independent (B_g) contributions. A spinodal model is an appropriate assumption here as the chemical composition of all alloys in this research are located very close to, or within, the spinodal line of the Fe-Cr miscibility gap [9]. Furthermore, it has previously also been found that alloys experiencing phase separation in the transient region can be modelled assuming a spinodal-like nanostructure [9]. The spinodal model used here is taken from the work of Furukawa [37] and is as follows:

$$I(Q)_{spinodal} = I_{peak}\left(1 + \frac{\gamma}{2}\right)x^2 / \left(\frac{\gamma}{2} + x^{2+\gamma}\right) \quad (3)$$

where, $x = Q/Q_{peak}$, Q_{peak} is the peak position and I_{peak} is the intensity at Q_{peak}. After fitting, values of the latter two parameters were extracted to describe the evolution of the phase separation. The term γ is equal to d + for off-critical concentration mixtures where the interface between different phases is relatively smoothly curved, and *2d* for critical concentration mixtures where the interface is entangled. A transition from $\gamma = d + 1$ to $\gamma = 2d$ is expected near the percolation threshold [37]. Here d is the dimensionality (*i.e.*, 1, 2, 3) of the system: 3 in this work. We have evaluated the goodness of fit using both $\gamma = 4$ (d + *1*) and $\gamma = 6$ (*2d*). In our previous studies [28, 33], we have used a value of $\gamma = 4$. However, here $\gamma = 6$ is chosen for all conditions – the assumption being the Cr concentration is close to the critical concentration. At the small length scales of interest, Furukawa [37] has already shown that it is natural that the fits are good with both assumptions ($\gamma = 4$ or 6) as interfaces may be smoothly curved even for critical concentrations. Furthermore, the goodness of fit obtained is good for all conditions when using $\gamma = 6$. Therefore, as all conditions are expected to decompose through spinodal decomposition or be in the transient region, we believe the assumption of a critical concentration mixture (above percolation threshold) and interconnected nanostructure to be reasonable.

Fits of Eq.2 to the SANS data (see Fig. 2) are very good, and the fitting parameters give information on the physical parameters of interest. This approach can accurately identify the changes in peak position and amplitude during the aging process. To obtain the corrected evolution of the scattering intensity shown in Fig. 3, the $I(Q)_{fit}$ in Fig. 2 was normalised by the background function B_{fit} (*i.e.*, $\frac{I(Q)_{fit}}{B_{fit}}$) to reveal the shape of the underlying spinodal signal (I_n). This "I_n" was then fitted to a Gaussian function $S(Q)_{fit}$ [16]. Signals of phase separation were then obtained by removing the contribution of the background and normalizing it with respect to B_{fit} *i.e.*, $S(Q) = B_{fit} * (S(Q)_{fit} - B_{fit}/B_{fit})$.

The distance between two α' domains *i.e.*, the wavelength of the spinodal decomposition can be obtained from the simple expression [16,17,19,27,28,36,38]:

$$\Lambda = 2\pi/Q_{peak} \quad (4)$$

With knowledge of Λ and the intensity of the spinodal peak, I_{peak}, the evolution of the amplitude of the concentration fluctuations within the ferrite phase of the 25Cr-7Ni super DSS can be extracted. Following Hashimoto et al. [39] and Meier and Strobl [40], and assuming the α' precipitate is a cube, we can define:

$$I_{peak} = \varphi\,(1-\varphi)\left(\frac{\Lambda}{2}\right)^3 (\Delta\rho)^2 \quad (5)$$

where, φ is the volume fraction of the α' phase in the ferrite and $\Delta\rho$ is the neutron scattering length density (SLD) difference between the α and α' phases. Then, from changes in the SLD we can obtain the changes in the Cr concentration, see Table 1 [35]. We note that the SLD of Fe-Cr binary alloys decrease by approximately 0.5×10^{-6} $Å^{-2}$ for every 10 at.% increase in Cr concentration and the amplitude (A at.%) can be obtained by:

$$\text{A (at.\%)} = \Delta\rho \frac{10 \text{ at.\%}}{0.5 \times 10^{-6} \forall^{-2}} \quad (6)$$

3. Results and discussion

The evolution of the scattering function with isothermal aging for Fe-36 wt.%Cr at 500 °C is shown in Fig. 3a. Here, peak intensity increased, and peak position moved towards lower Q (longer Λ) with increase in isothermal aging time. To validate our SANS quantification approach, we compare the quantifications performed on Fe-Cr alloys in the present

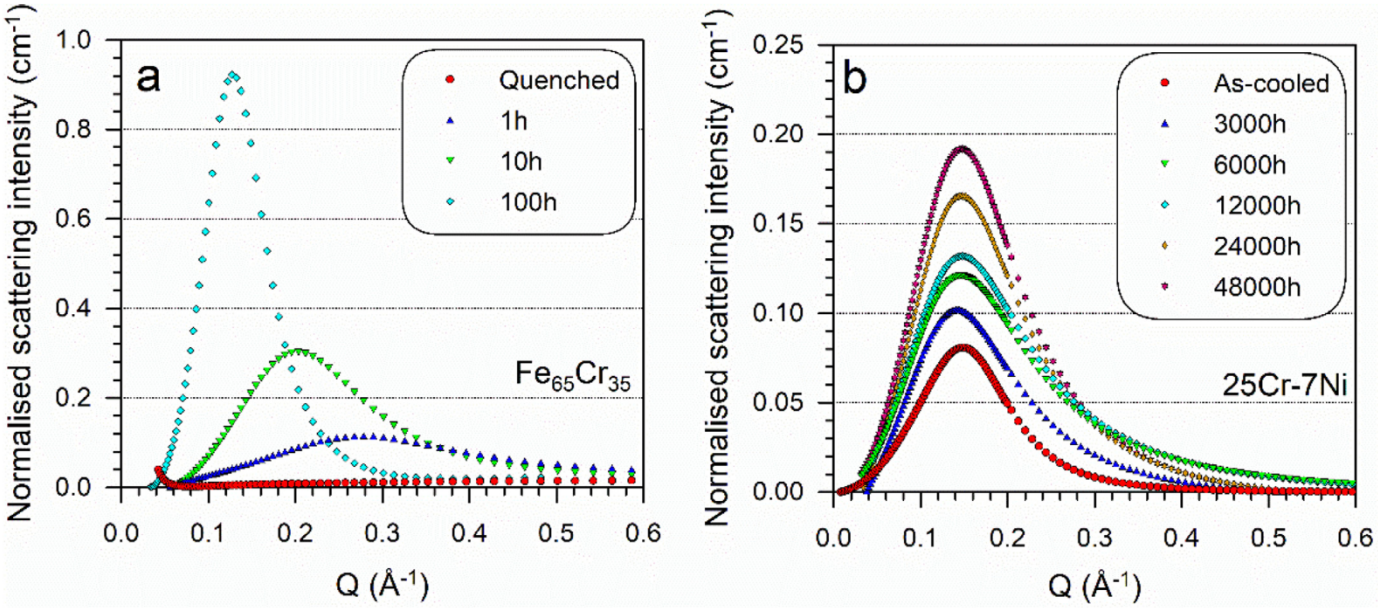

Fig. 3. a) Normalised total scattering intensity evolution during the isothermal aging of $Fe_{65}Cr_{35}$ at 500 °C. b) Normalised nuclear scattering intensity evolution during the isothermal aging of 25Cr-7Ni super DSS at 300 °C. normalization of scattering according to Ref. [11] but using the fitted background for subtraction.

Table 1
Neutron SLD values of Fe-Cr binary alloys (values computed for neutron λ=6 Å) [35].

Serial number	Material	Density (g/cm^3)	Neutron SLD (× 10^{-6}/Å^2)
1	Fe	7.87	8.02
2	Cr	7.19	3.03
3	$Fe_{90}Cr_{10}$	7.81	7.49
4	$Fe_{80}Cr_{20}$	7.74	6.96
5	$Fe_{75}Cr_{25}$	7.70	6.70
6	$Fe_{70}Cr_{30}$	7.67	6.44
7	$Fe_{65}Cr_{35}$	7.63	6.18
8	$Fe_{60}Cr_{40}$	7.60	5.93
9	$Fe_{50}Cr_{50}$	7.53	5.42
10	$Fe_{40}Cr_{60}$	7.46	4.93
11	$Fe_{30}Cr_{70}$	7.40	4.44
12	$Fe_{20}Cr_{80}$	7.33	3.96
13	$Fe_{10}Cr_{90}$	7.26	3.49

work with APT quantifications from the literature [11,28]. Table 2 indicates that the quantification of the wavelength from SANS is in good agreement with the APT data from the literature. However, the SANS data here is judged as more accurate considering that a much larger volume was sampled in addition to its being a more reliable measurement method for probing the length-scale of concentration correlations. APT is inherently sensitive to evaporation trajectory aberrations and 3D reconstruction errors. In the case of amplitude, the data from literature was assessed by radial distribution function (RDF) analysis [11] and the Langer-Bar-on-Miller (LBM) method [41,42], see Table 2.

For the binary Fe-Cr alloys it was necessary to consider the proportions of nuclear scattering and magnetic scattering since a saturating magnetic field was not applied during the measurements. When the nuclear scattering was not deconvoluted from the total scattering the question arises as to how much of the spinodal peak is due to magnetic scattering. In the early stage of phase separation it has been found that magnetic scattering is negligible, while the nuclear and magnetic scattering are approximately equal for longer aging times, *i.e.*, for late stages of phase separation [33,43]. This information has been used in the present work, *i.e.*, in early stage of decomposition $I_{nuclear} \approx I_{total}$, whereas in the late stages of decomposition $I_{nuclear} \approx I_{magnetic} \approx 0.5\ I_{total}$.

Furthermore, we evaluated the amplitude using two different assumptions for the volume fraction of *α'*. Firstly, the volume fraction was assumed to be *0.5*. This is believed to be a reasonable assumption in the case of sinusoidal spinodal fluctuations around the mean ferrite composition in the early stage of phase separation [44], but in the case of off-critical Cr compositions an asymmetric nanostructure (unequal phase fractions of *α* and *α')* would develop over time, and after long term aging the equilibrium phase fractions would be reached. In such a case, the second assumption of an equilibrium volume fraction ($\varphi = \varphi_{eq.}$), calculated using the Thermo-Calc Software TCFE9 Steels/Fe-alloys database [45] would be more appropriate. This second assump-

Table 2
Comparison of wavelength and amplitude values for Fe1-x-Crx derived from SANS measurements (this work: SANS data from previous beamtime as reported [29]) and APT results from the literature. Isothermal aging experiments were done ex situ at 773 K (500 °C) [11,28].

Alloy	Aging Time (h)	$\varphi_{\alpha'}$ TC-eq.	χ^2	Λ (nm) This work	Λ (nm) Literature	A (at.%) This work $\varphi = 0.5$	A (at.%) This work $\varphi = eq.$	A (at.%) -RDF Literature	A(at.%)-LBM Literature
Fe-36Cr	1	0.28	9.9	2.5	3.0	25.6	28.6	13.6	–
Fe-36Cr	10	0.28	9.7	3.2	3.6	27.4	30.7	20.1	10.7
Fe-36Cr	100	0.28	13.9	5.3	5.6	36.2	40.5	35.4	17.7
Fe-30Cr	20	0.20	5.7	3.0	3.3	24.6	30.8	16.6	9.3
Fe-30Cr	200	0.20	9.3	5.1	5.4	34.9	43.6	43.8	19.2
Fe-25Cr	100	0.12	5.5	3.6	4.0	21.6	32.7	17.5	9.5
Fe-25Cr	1000	0.12	12.5	7.4	7.8	34.6	52.5	54	23.4

Table 3
APT and SANS comparison of decomposition wavelength and amplitude for 25Cr-7Ni DSS obtained in this work in comparison to the work of Pettersson et al. [34]. (TC-equilibrium: φ=0.25).

Serial Number	Aging Time (hrs)	Λ (nm) APT Pettersson et al. [34]	Amplitude (at.%) APT - RDF	χ^2 $-20° \leq \Psi \leq +20°$	Λ (nm) SANS	Amplitude (at.%) (φ = 0.5) SANS	Amplitude (at.%) (φ = *eq.*) SANS
1	0	4	15.6	1.2	5.1	15.0	17.3
2	3000	4	15.8	1.3	4.8	16.8	19.4
3	6000	4	17.2	1.7	4.7	18.3	21.1
4	12,000	4	18.4	1.5	4.6	18.6	21.5
5	24,000	–	–	1.4	4.7	20.1	23.2
6	48,000	–	–	3.0	4.5	33.4	38.6

tion is also believed to be more appropriate when the phase separation occurs via nucleation and growth, when it is more appropriate to assume that the α' phase nucleated and grown in the early stages is equal or below the equilibrium phase fraction of α'. These two assumptions are evaluated on the aged binary Fe-Cr alloys in the present work and it is found that there is good agreement with the description above. This means that the quantification of amplitude for all three binary Fe-Cr alloys are in good agreement with APT-RDF quantification in the early stage of decomposition when using the first assumption, *i.e.* $\varphi = 0.5$. For off-critical compositions and longer aging times the second assumption, *i.e.*, $\varphi_{eq.}$ seems to provide better agreement of amplitude with APT-RDF quantifications. The results for different $\varphi_{\alpha'}$ are presented in Table 2. Table 2 shows that there are no significant differences between the two assumptions for relatively early stages of phase separation, which are both slightly higher than the RDF and LBM amplitudes, *e.g.*, Fe-35Cr alloy after aging for 1 h and Fe-30Cr after aging for 20 h. As the aging time increases *e.g.*, Fe-35Cr aged for 100 h, Fe-25Cr aged for 100 h, the amplitude values (for $\varphi = 0.5$) become closer to RDF results. However, for the longest aging times where decomposition was severe *e.g.*, Fe-30Cr aged for 200 h, Fe-25Cr aged for 1000 h, it was the equilibrium assumption ($\varphi_{eq.}$) that are closer to APT-RDF amplitudes. These analyses of the binary Fe-Cr alloys suggests that the assumption $\varphi = 0.5$ should be used for all ageing conditions of the 25Cr-7Ni super DSS, since it is assumed to decompose through spinodal decomposition and all conditions should represent the early stage of phase separation.

In all, for the binary Fe-Cr alloys, there was a good agreement between the SANS derived quantities and the APT analysis using the RDF method. However, the comparison between LBM in APT and the SANS quantification of amplitude was worse – the LBM method indicated significantly lower amplitudes. It has been argued in the literature that the RDF approach is a more accurate way to evaluate amplitude (the peak to trough) of phase separation from APT [11]. Whereas, the LBM approach which only considers the center of Gaussian distributions may underestimate the spinodal amplitude [11]. In simple terms, the RDF method better captures the center of the Cr-rich α' domains, whereas the LBM method is more close to the average difference of the Fe-rich α and Cr-rich α' domains.

Having ascertained that the SANS evaluation method is robust, the same approach was applied to the study of the industrially relevant 25Cr-7Ni super DSS. The SANS data is presented in Fig. 3b. The signature of phase separation in the reference condition is believed to be a consequence of exposure in the miscibility gap during manufacturing of the alloy. In Table 3 the SANS quantifications are compared with the APT-RDF results of Pettersson et al. [34]. Only the nuclear scattering contribution is considered in the analysis since this can be directly related to the concentration amplitude.

With increase in isothermal aging time, there was a noticeable increase in the nuclear scattering contributions, which implied that α and α' phase separation was becoming more pronounced [33]. Similar to the results from *Fe-Cr* in Table 2, we can also confirm that for the 25Cr-7Ni super DSS (see Fig. 4) the assumption that $\varphi = 0.5$ was suitable for the early stage of phase separation appears valid. Note: here it is the volume fraction of α' with respect to the ferrite phase in the 25Cr-7Ni super DSS, *i.e.*, fifty percent in 40.6 vol.% ferrite. Moreover, there is APT-RDF data to compare with for up to 12,000 h of aging, and since the amplitude evolution is quite minor until 48,000 h, we believe the same assumption is valid for all the conditions in the present work. For the first 12,000 h of aging, the difference in amplitude from the nuclear scattering was ~ 3.6 at.%, whereas the difference in amplitude evaluated by the RDF method from APT results was ~ 2.8 at.%. Here it can be seen that the amplitude assessed from SANS is in very good agreement with APT-RDF results, both in terms of values and relative differences (see Fig. 4). One uncertainty that is worth noting here is that we only attribute the difference in scattering peak intensity to the Cr fluctuations (see Eq. (6)), but in reality when aging 25Cr-7Ni super DSS for long time, there should also be small differences in the partitioning of other alloying elements such as Ni, Mn *etc.* [46] which will also contribute to the change of the SLD. However, we have calculated that the Cr signal is about 5 times that of the next most significant element Mn. The good agreement with APT-RDF results further indicates that the assumption in the present work of relating the SLD difference only to Cr appears reasonable, since all conditions are early stage of phase separation. The nuclear scattering contributions from SANS provided a sensitive measure of the amplitude and another advantage of the SANS technique was that it was more sensitive to changes in the wavelength of α and α' phase separation in comparison to the APT method. From Fig. 4, it is evident that SANS technique observed subtle changes in the wavelength of decomposition during the early stages of the α and α' phase separation which APT–RDF analysis did not. It should be noted that the APT–RDF analysis is a simplified approach for the wavelength determination. It can also be noted that the quantification of amplitude seems to be more accurate for the super DSS as compared to the binary Fe-Cr alloys in the present work. This is likely an effect of the simplified deconvolution of nuclear scattering for the binary Fe-Cr alloys.

The amplitude and minute nanostructural wavelength fluctuations during α and α' phase separation has a marked effect on the changes to the mechanical properties of the 25Cr-7Ni super DSS. Fig. 5 shows the micro-hardness measurements for the austenite and ferrite phases as well as the Charpy-V impact toughness measurements, *i.e.*, the energy absorbed in Joules for the alloy. From Fig. 5, it is clear that the hardness of the ferrite phase increases, and the energy absorbed continuously decreases with increase in the isothermal aging time. This clearly indicates that even though the wavelength of the concentration fluctuations decreases slightly from 5.1 nm to 4.5 nm, and the increase of amplitude is only ~ 18.4 at.%, these changes to the nanostructure, cause significant changes to the micro-hardness of the ferrite phase and correspondingly the impact energy of the 25Cr-7Ni super DSS was dramatically reduced. We note that only a few reports in the literature on the topic do consider these early stages of the decomposition process *e.g.*, the work of Tucker *et al.* [47], yet this is where the technical interest lies. Here as well, we clearly show that these changes in structure of the materials at the *nanometer* length scales are the underlying reason for the continuous and dramatic changes in hardness

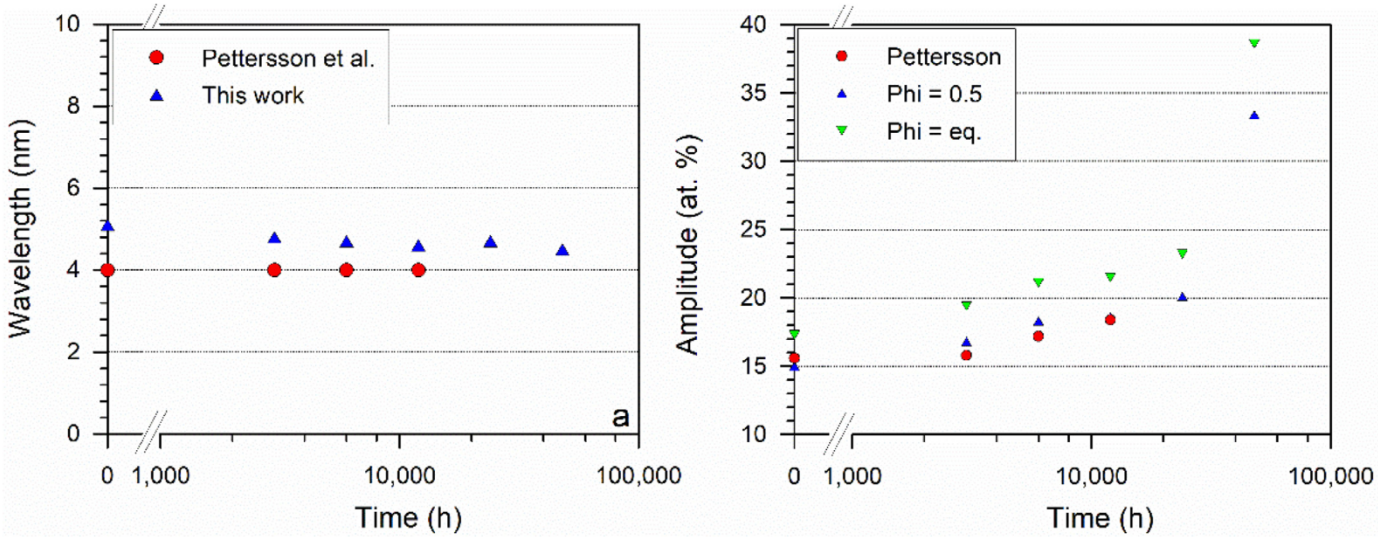

Fig. 4. APT and SANS comparison of (a) decomposition wavelength and (b) decomposition amplitude for 25Cr-7Ni DSS obtained in this work in comparison to the APT work of Pettersson et al. [34]. (TC-equilibrium: φ=0.25).

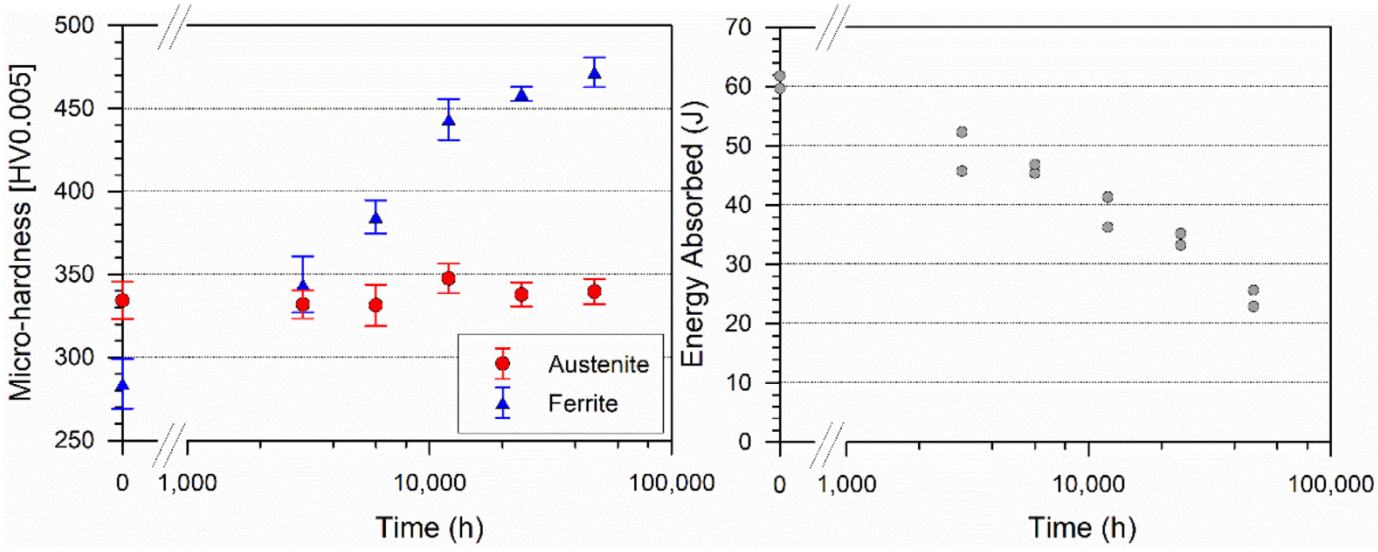

Fig. 5. a. Micro-hardness evolution of austenite and ferrite for isothermally aged 25Cr-7Ni super DSS at 300 °C. b. Charpy-V impact energy absorbed values in Joules for isothermally aged 25Cr-7Ni super DSS at 300 °C.

and toughness, even during the early stages of phase separation process. Further work should focus on a systematic mapping of the decomposition and the correlated embrittlement in a variety of commercial grade DSS exposed to relevant long-term aging temperatures and times.

4. Conclusions

This work presents a small-angle neutron scattering approach for quantitatively analysing nanostructural features such as the amplitude and wavelength of α and α' phase separation phenomena in binary Fe-Cr alloys and 25Cr-7Ni (wt.%) commercial grade super duplex stainless steel, particularly during the early stages of the phase separation process. Where possible, the amplitude and wavelength values have been compared with similar data from atom probe tomography (APT) measurements present in the literature. It was found that the amplitude and wavelength measured by both techniques have good agreement.

The key observation on the isothermal aging of 25Cr-7Ni super duplex stainless steel at 300 °C was that the relatively minor decomposition that takes place up until 48 000 h (characterised by a wavelength decrease from 5.1 to 4.5 nm and amplitude increase from 15.0 to 33.4 at.%) led to a pronounced hardening of the ferrite phase by 190 HV and a reduction of the sub-size Charpy-V impact toughness from 60 J to 25 J. Future endeavours should focus on applying the high-throughput quantitative analysis method presented here to evaluate nanostructural evolution of duplex stainless steel and subsequently use this information as input parameters for material models to study and predict evolution in mechanical properties. These studies should focus on structure and property evolution at the early stages of embrittlement for industrially relevant aging conditions *i.e.* long-term aging at intermediate and low temperatures.

Declaration of Competing Interest

The authors declare that they have no known competing financial interests or personal relationships that could have appeared to influence the work reported in this paper.

Acknowledgements

The project COOLER was financed by VINNOVA under contract 2015–03453 within the Strategic Swedish Innovation Programme for Metallic Materials 2013–2016 and the participating companies Forsmarks Kraftgrupp AB, Haldor Topsoe A/S, OKG AB, Outokumpu Stainless AB and Ringhals AB. The Vinnova COOLER LSI project is also acknowledged for financial support. JL would like to thank the China Scholarship Council (CSC No.201700260207) for financial support. YD would like to thank Dr Hossein Ehteshami for his valuable discussions and suggestions during the writing of this manuscript. YD would also like to acknowledge the award of an Olle Eriksson travel grant. The authors would like to thank the UK Science & Technology Facilities Council, part of UK Research & Innovation, for the award of neutron beamtime (Experiment RB1810590) at the ISIS Pulsed Neutron & Muon Source. This work benefited from the use of the SasView application, originally developed under NSF Award DMR-0520547. SasView also contains code developed with funding from the EU Horizon 2020 program under the SINE2020 project Grant No. 654000.

References

[1] F. Danoix, P. Auger, Atom probe studies of the Fe-Cr system and stainless steels aged at intermediate temperature: a review, Mater. Charact. 44 (1–2) (2000) 177–201.
[2] S. Brenner, M. Miller, W. Soffa, Spinodal decomposition of iron-32 at.% chromium at 470°C, Scr. Metall. 16 (7) (Jul. 1982) 831–836.
[3] S. Katano, M. Iizumi, Crossover phenomenon in dynamical scaling of phase separation in Fe-Cr alloy, Phys. Rev. Lett. 52 (10) (1984) 835–838.
[4] S. Katano, M. Iizumi, Decomposition kinetics in iron-chromium alloys, Phys. B+C 120 (1–3) (1983) 392–396.
[5] S. Spooner, W.E. Brundage, Isotropy of Spinodal decomposition in Fe-30% Cr, Scr. Metall. 17 (4) (1983) 573–574.
[6] J. Zhou, J. Odqvist, L. Höglund, M. Thuvander, T. Barkar, P. Hedström, Initial clustering - A key factor for phase separation kinetics in Fe-Cr-based alloys, Scr. Mater. 75 (2014) 62–65.
[7] M.K. Miller, J.M. Hyde, A. Cerezo, G.D.W. Smith, Comparison of low temperature decomposition in Fe-Cr and duplex stainless steels, Appl. Surf. Sci. 87–88 (1995) 323–328.
[8] R.O. Williams, The miscibility gap in the iron-chromium system, Metall. Trans. 5 (April) (1974) 967–968.
[9] W. Xiong, M. Selleby, Q. Chen, J. Odqvist, Y. Du, Phase Equilibria and Thermodynamic Properties in the Fe-Cr System, Crit. Rev. Solid State Mater. Sci. 35 (2) (2010) 125–152.
[10] C. Pareige, et al., Kinetic study of phase transformation in a highly concentrated Fe-Cr alloy: Monte Carlo simulation versus experiments, Acta Mater. 59 (6) (2011) 2404–2411.
[11] J. Zhou, J. Odqvist, M. Thuvander, P. Hedström, Quantitative evaluation of spinodal decomposition in Fe-Cr by atom probe tomography and radial distribution function analysis, Microsc. Microanal. 19 (03) (Jun. 2013) 665–675.
[12] O. Tissot, et al., Comparison between SANS and APT measurements in a thermally aged Fe-19 at.%Cr alloy, Mater. Charact. 151 (2019) 332–341 October 2018.
[13] X. Xu, et al., Effect of cooling rate after solution treatment on subsequent phase separation during aging of Fe-Cr alloys: a small-angle neutron scattering study, Acta Mater. 134 (2017) 221–229.
[14] X. Xu, J.E. Westraadt, J. Odqvist, T.G.A. Youngs, S.M. King, P. Hedström, Effect of heat treatment above the miscibility gap on nanostructure formation due to spinodal decomposition in Fe-52.85 at.%Cr, Acta Mater. 145 (2018) 347–358.
[15] S.A. Briggs, et al., A combined APT and SANS investigation of α' phase precipitation in neutron-irradiated model FeCrAl alloys, Acta Mater. 129 (2017) 217–228.
[16] M. Hörnqvist, M. Thuvander, A. Steuwer, S. King, J. Odqvist, P. Hedström, Early stages of spinodal decomposition in Fe-Cr resolved by in-situ small-angle neutron scattering, Appl. Phys. Lett. 106 (6) (2015) 1–5.
[17] F. Bley, Neutron small-angle scattering study of unmixing in FeCr alloys, Acta Metall. Mater. 40 (7) (1992) 1505–1517.
[18] H.D. Solomon, L.M. Levinson, Mossbauer effect study of '475°C embrittlement' of duplex and ferritic stainless steels, Acta Metall. 26 (3) (1978) 429–442.
[19] T. de Nys, P.M. Gielen, Spinodal decomposition in the Fe-Cr system, Metall. Trans. 2 (5) (1971) 1423–1428.
[20] D. Chandra, L.H. Schwartz, Mossbauer Effect Study of the 475°C Decomposition of Fe-Cr, Metall. Trans. 2 (2) (1971) 511–519.
[21] J.E. Westraadt, et al., A high-resolution analytical scanning transmission electron microscopy study of the early stages of spinodal decomposition in binary Fe–Cr, Mater. Charact. 109 (2015) 216–221.
[22] O. Soriano-Vargas, E.O. Avila-Davila, V.M. Lopez-Hirata, N. Cayetano-Castro, J.L. Gonzalez-Velazquez, Effect of spinodal decomposition on the mechanical behavior of Fe-Cr alloys, Mater. Sci. Eng. A 527 (12) (2010) 2910–2914.
[23] L. Couturier, F. De Geuser, A. Deschamps, Direct comparison of Fe-Cr unmixing characterization by atom probe tomography and small angle scattering, Mater. Charact. 121 (2016) 61–67.
[24] L. Couturier, F. De Geuser, A. Deschamps, Microstructural evolution during long time aging of 15–5PH stainless steel, Materialia 9 (February) (2020) 100634.
[25] M. Guttmann, Intermediate temperature aging of duplex stainless steels. A review, in: Proceedings of the Duplex Stainless Steel Conference, 1991, pp. 79–92.
[26] SVENSK STANDARD, Metallic materials – Charpy pendulum impact test – Part 3: preparation and characterization of Charpy V-notch test pieces for indirect verification of pendulum impact machines (SS-EN ISO 148-3:2008), no. 121687. Sweden, 2008.
[27] R.K. Heenan, J. Penfold, S.M. King, SANS at pulsed neutron sources: present and future prospects, J. Appl. Crystallogr. 30 (6) (1997) 1140–1147.
[28] X. Xu, S. Wessman, J. Odqvist, S.M. King, P. Hedström, Nanostructure, microstructure and mechanical properties of duplex stainless steels 25Cr-7 Ni and 22Cr-5Ni (wt.%) aged at 325°C, Mater. Sci. Eng. A 754 (March) (2019) 512–520.
[29] X. Xu, et al., Structural characterization of phase separation in Fe-Cr: a current comparison of experimental methods, Metall. Mater. Trans. A 47A (12) (2016) 5942–5952.
[30] O. Arnold, et al., Mantid - data analysis and visualization package for neutron scattering and μ SR experiments, Nucl. Instrum. Methods Phys. Res. Sect. A Accel. Spectrom. Detect. Assoc. Equip. 764 (2014) 156–166.
[31] "Mantid Project Version 4.2." [Online]. Available: https://www.mantidproject.org/Main_Page. [Accessed: 13-Jan-2020].
[32] G.D. Wignall, F.S. Bates, Absolute calibration of small-angle neutron scattering data, J. Appl. Crystallogr. 20 (1987) 28–40.
[33] X. Xu, J. Odqvist, S.M. King, D. Alba Venero, P. Hedström, Nuclear and magnetic small-angle neutron scattering in self-organizing nanostructured Fe_(1-x)–Cr_x alloys, Mater. Charact. 164 (December 2019) (Jun. 2020.) 110347.
[34] N. Pettersson, et al., Nanostructure evolution and mechanical property changes during aging of a super duplex stainless steel at 300°C, Mater. Sci. Eng. A 647 (2015) 241–248.
[35] "SasView Version 4.2.2" [Online]. Available: http://www.sasview.org [Accessed: 01-Jan-2020].
[36] B. Hammouda, "Probing Nanoscale Structures - The SANS Toolbox" [Online]. Available: https://www.ncnr.nist.gov/staff/hammouda/the_SANS_toolbox.pdf. [Accessed: 01-Jan-2020].
[37] H. Furukawa, Dynamics-scaling theory for phase-separating unmixing mixtures: growth rates of droplets and scaling properties of autocorrelation functions, Phys. A Stat. Mech. Appl. 123 (2–3) (1984) 497–515.
[38] D.L. Price, F. Fernandez-Alonso, An Introduction to Neutron Scattering, in: Experimental Methods in the Physical Sciences, 44, 1st ed., Elsevier Inc., 2013, pp. 1–136.
[39] T. Hashimoto, M. Takenaka, H. Jinnai, Scattering studies of self-assembling processes of polymer blends in spinodal decomposition, J. Appl. Crystallogr. 24 (pt 5) (1991) 457–466.
[40] H. Meier, G.R. Strobl, Small-angle x-ray scattering study of spinodal decomposition in polystyrene/poly(styrene-co-bromostyrene) blends, Macromolecules 20 (3) (1987) 649–654.
[41] J.S. Langer, M. Bar-on, H.D. Miller, New computational method in the theory of spinodal decomposition, Phys. Rev. A 11 (1975) 1417–1429.
[42] M.K. Miller, Atom Probe Tomography and the Local Electrode Atom Probe, vol. c, no. 1994. 2000.
[43] J.C. Lasalle, L.H. Schwartz, Further studies of spinodal decomposition in Fe-Cr, Acta Metall. 34 (6) (1986) 989–1000.
[44] K. Binder, P. Fratzl, Spinodal decomposition, in: Proceedings of the IUPAC Compendium of Chemical Terminology, 2015 April 2006.
[45] Thermo-Calc, "TCFE9: TCS steel and Fe-alloys database extended information," Thermo Calc., pp. 1–44.
[46] J. Zhou, J. Odqvist, M. Thuvander, S. Hertzman, P. Hedström, Concurrent phase separation and clustering in the ferrite phase during low temperature stress aging of duplex stainless steel weldments, Acta Mater. 60 (16) (2012) 5818–5827.
[47] Tucker, Assessment of thermal embrittlement in duplex stainless steels 2003 and 2205 for nuclear power applications, Acta Materialia (2015), doi:10.1016/j.actamat.2014.12.012.